nature biotechnology

Energy extraction from the biologic battery in the inner ear

Patrick P Mercier[1,5,6], Andrew C Lysaght[2,3,6], Saurav Bandyopadhyay[1,6], Anantha P Chandrakasan[1,7] & Konstantina M Stankovic[2–4,7]

Endocochlear potential (EP) is a battery-like electrochemical gradient found in and actively maintained by the inner ear[1,2]. Here we demonstrate that the mammalian EP can be used as a power source for electronic devices. We achieved this by designing an anatomically sized, ultra-low quiescent-power energy harvester chip integrated with a wireless sensor capable of monitoring the EP itself. Although other forms of *in vivo* energy harvesting have been described in lower organisms[3–5], and thermoelectric[6], piezoelectric[7] and biofuel[8,9] devices are promising for mammalian applications, there have been few, if any, *in vivo* demonstrations in the vicinity of the ear, eye and brain. In this work, the chip extracted a minimum of 1.12 nW from the EP of a guinea pig for up to 5 h, enabling a 2.4 GHz radio to transmit measurement of the EP every 40–360 s. With future optimization of electrode design, we envision using the biologic battery in the inner ear to power chemical and molecular sensors, or drug-delivery actuators for diagnosis and therapy of hearing loss and other disorders.

Implantable electronics for medical applications typically require large energy reservoirs to operate reliably over long periods of time. In both human health care and animal studies, anatomy often limits the size of implantable batteries, requiring surgical reimplantation or cumbersome external wireless power sources for long-term operation. Harvesting energy from nearby energy sources is an alternative approach to extend implant life and, with sufficient available energy, to allow the implant to operate autonomously. As humans and animals already generate and consume a vast amount of power[10], biologically based energy harvesting is a potential solution to power implanted devices. However, some biological energy sources, such as heat captured using thermoelectric devices[6], and muscle movements captured using piezoelectric devices or induction generators[11], are not suitable for mammalian implantable applications as they require externally worn apparatuses. Meanwhile, previous reports of large-scale biofuel cells have long-term stability challenges[12], or extract power from living trees[3], neither of which is a suitable source for implantable medical devices. Among the *in vivo* biological energy sources reported, the potential of a microbial glucose fuel cell has been found to be 0.2–0.62 V (ref. 8), whereas that of a cockroach is 0.2–0.25 V (ref. 4), and of a snail is 0.53 V (ref. 5). Although quite promising, these potentials are not generated in mammals or are difficult to extract in anatomically sized *in vivo* devices.

At 70–100 mV, the EP is the largest positive direct current electrochemical potential in mammals. (Although animal resting potentials can vary between −20 and −120 mV, such potentials occur at the cellular level and are not available in such a large reservoir.) The EP is the main driving force for cochlear mechanotransduction of sound pressure vibrations to neurotransmitter release and excitation of the auditory nerve. Although the EP is well understood and modeled[2,13,14], to our knowledge it has never been harvested to drive electronics. Its inherent stability over mammalian lifetimes[15] makes it a candidate for powering long-term, energy-autonomous implantable devices. The EP arises from the difference in ionic concentration between endolymph—an extracellular fluid in the inner ear—and perilymph, an extracellular fluid that bathes surrounding spaces. Endolymph, which has a higher potassium concentration than that inside cells or in perilymph, is separated from perilymph by a complex network of tight junctions (**Fig. 1**). The EP effectively acts as a biologic battery whose potential is actively stabilized by potassium channels, pumps and cotransporters (**Fig. 2**) in cells of the stria vascularis, a specialized structure that borders the endolymphatic space.

Any electronic system that interfaces with and extracts power from the EP should not interfere with the normal function of the cochlea. Total current flow through the guinea pig cochlea (including both sensory and nonsensory cells), whose anatomy and physiology is similar to that of humans, has previously been determined to be 0.8–1.6 μA per millimeter of cochlear wedge[16]. Given the 18-mm length of the guinea pig cochlea[17], currents generated by the stria vascularis on the order of 14–28 μA occur in the guinea pig physiologically and place an upper limit on extractable electric current from the cochlea.

In practice, the maximum current extractable from the EP by an implanted energy harvester is constrained well below this limit by the high-impedance electrodes that we used, which had

[1]Microsystem Technology Laboratories, Massachusetts Institute of Technology, Cambridge, Massachusetts, USA. [2]Eaton Peabody Laboratory and Department of Otolaryngology, Massachusetts Eye and Ear Infirmary, Boston, Massachusetts, USA. [3]Program in Speech and Hearing Bioscience and Technology, Harvard/Massachusetts Institute of Technology Joint Division of Health Sciences and Technology, Cambridge, Massachusetts, USA. [4]Department of Otology and Laryngology, Harvard Medical School, Boston, Massachusetts, USA. [5]Present address: Department of Electrical and Computer Engineering, University of California, San Diego, La Jolla, California, USA. [6]These authors contributed equally to this work. [7]A.P.C. and K.M.S. jointly supervised this work. Correspondence should be addressed to A.P.C. (anantha@mtl.mit.edu) or K.M.S. (konstantina_stankovich@meei.harvard.edu).

Received 23 July; accepted 18 September; published online 8 November 2012; doi:10.1038/nbt.2394

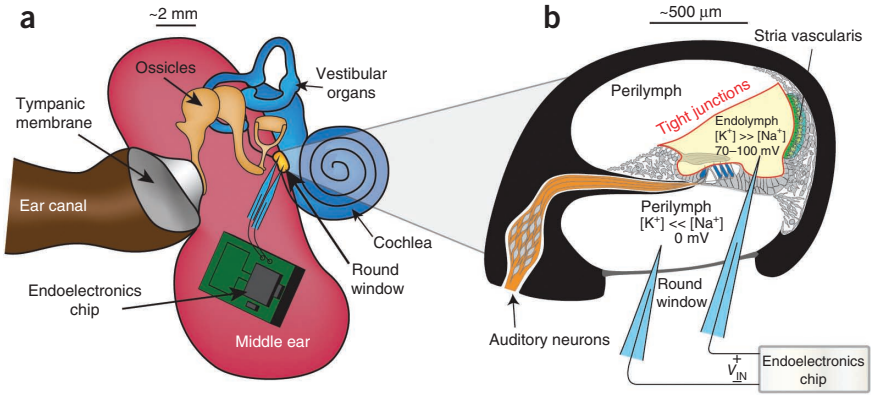

Figure 1 Anatomy and physiology of the inner ear. (**a**) Schematic of a mammalian ear including the external, middle and inner ear, which contains the cochlea and vestibular end organs. The endoelectronics chip is illustrated in one possible location, although the experiments were done with the chip located outside of the middle ear cavity. (**b**) Cross-section of a typical cochlear half-turn, showing the endolymphatic space (yellow) bordered by tight junctions (red), the stria vascularis (green) and hair cells (blue), which are contacted by primary auditory neurons (orange).

sharp tips so as to minimize cell damage when they are inserted into the EP space. The input power to the implantable energy harvester, which we refer to as the endoelectronics chip, is given as

$$P = V_{IN}^2/R_{in,eff} = [V_{EP}/(R_{in,eff} + R_{elec})]^2 \times R_{in,eff}$$

where V_{EP} is the endocochlear potential, R_{elec} and $R_{in,eff}$ are the impedances of the glass electrodes and the endoelectronics chip, respectively, and V_{IN} (equal to $V_{EP}R_{in,eff}/(R_{in,eff} + R_{elec})$) is the effective input voltage to the endoelectronics chip (**Fig. 2**). Given electrode impedance constraints, the extractable power is maximized when $R_{in,eff}$ is configured close to R_{elec}. For the glass microelectrodes traditionally used, the tradeoff between electrode impedance and bluntness reaches a point of diminishing returns at R_{elec} = 0.4–1.1 MΩ, when a further increase in the diameter of the electrode tip (that is, bluntness) increases collateral cell damage during insertion while not offering a substantially lower impedance. This results in extractable power ranging from 1.1–6.3 nW with V_{IN} in the range of 30–55 mV.

The low EP voltage, in conjunction with the low extractable power, poses two substantial challenges for harvesting net positive energy. First, transistor-based electronics require hundreds of millivolts to start up in the absence of expensive semiconductor post-processing[18,19]. Second, the maximum extractable power levels are at least an order of magnitude less than the quiescent power of the most efficient energy-harvesting and energy-sensing circuits in the literature[20–22]. For continuous, self-sustaining operation, quiescent (that is, standby) power should be well below the maximal extractable power.

We overcame the challenges of energy harvesting from the EP with a custom integrated circuit featuring a wireless kick-start energy receiver and energy buffering power electronics that consume at least an order of magnitude lower power than previous work[19–21]. The low-voltage turn-on issue was addressed by delivery of an initial one-time wireless start-up charging packet[23] of less than 2 s between an external radio frequency source and an on-board 3 × 4 mm^2 loop antenna. This charging packet was converted from radio frequency power to direct current to charge a 200-nF energy buffer capacitor, C_{supply} (**Fig. 2**), up to a maximum of 1.4 V. At such a voltage, C_{supply} contained up to 200 nJ, which was sufficient to operate the system for at most 6 min before the stored energy was completely exhausted (given a total system power consumption of 573 pW, as discussed below). To sustain the charge on C_{supply} once the external radio frequency source was removed, we used a boost converter to harvest the low-voltage EP energy by transferring and converting this energy to a higher voltage suitable for buffering energy onto C_{supply}. For system sustainability, the quiescent power consumption of the circuits that control the boost converter should be much less than the available output power. We implemented a continuously running timer and driver circuits that consumed 527 pW at 0.9 V, controlling the boost converter and activating a load circuit every 40–360 s. The boost converter achieved an efficiency of 53.4%. After including the timer and driver overhead, 60–2,840 pW of net positive power was extracted and available for the load circuit.

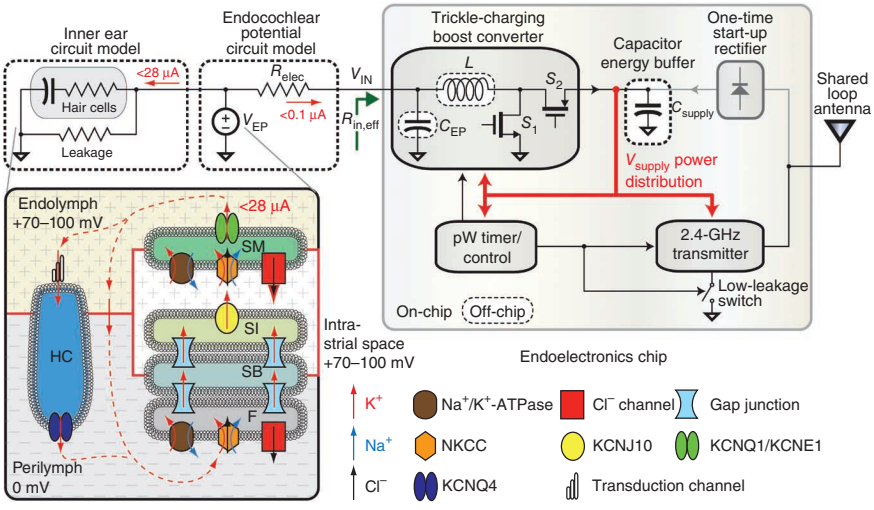

Figure 2 Schematic of the endoelectronics chip and equivalent circuit model of the endocochlear potential and inner ear tissues. To generate and maintain the EP, perilymphatic K^+ enters fibrocytes (F) via Na^+/K^+-ATPase and Na-K-Cl cotransporter. Gap junction networks connect fibrocytes to strial basal (SB) and intermediate (SI) cells, allowing ions to enter the intrastrial space via KCNJ10 channels. Strial marginal (SM) cells uptake K^+ against a substantial concentration gradient and release K^+ into endolymph. K^+ returns to perilymph either by entering hair cells (HC) apically during mechanoelectrical transduction of sound and exiting basolaterally via KCNQ4 channels, or via leakage current through the surrounding tissues (solid red lines represent tight-junction networks). With energy from the EP, a boost converter was used to trickle-charge capacitor C_{supply}, which supplies power to an integrated wireless transmitter. Switch S_1 in the converter was used to temporarily store energy in the inductor (L), and switch S_2 was used to transfer the stored energy onto C_{supply} at the higher required voltage. Once C_{supply} had stored sufficient energy, the transmitter entered its active mode and wirelessly transmitted a packet to a nearby receiver, after which it returned to a low-leakage standby mode and the boost converter began to replenish C_{supply}. A start-up rectifier was used with an external wireless power source to initialize the system.

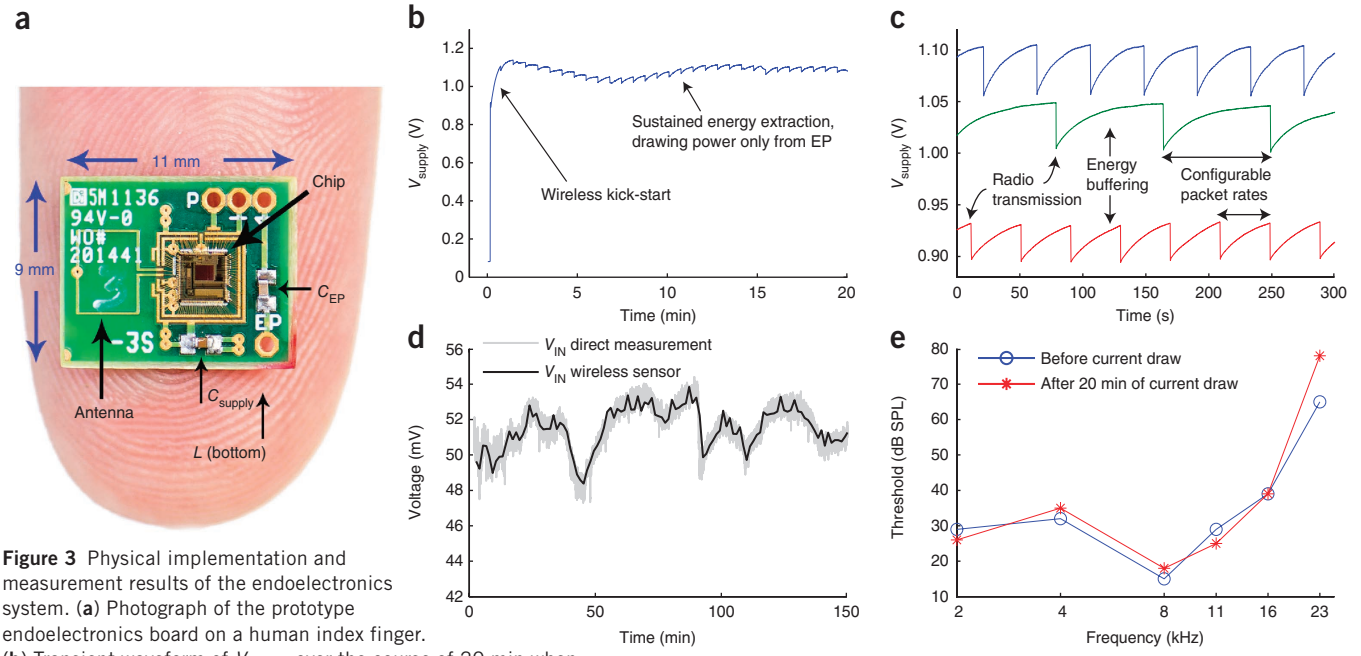

Figure 3 Physical implementation and measurement results of the endoelectronics system. (**a**) Photograph of the prototype endoelectronics board on a human index finger. (**b**) Transient waveform of V_{supply} over the course of 20 min when operating with a guinea pig EP as the only source of energy into the system (apart from the initial wireless kick-start). (**c**) Transient waveform of V_{supply} for three different experiments on three different animals. A 300-s timescale is used to show C_{supply} charging from the boost converter harvesting EP energy, as well as rapid periodic discharging from wireless transmissions. (**d**) Measurement of V_{IN}, which is a measurement of EP after a voltage drop across the electrode impedance. The black line represents measurements by an external device powered by a battery, whereas the gray line is the V_{IN} estimate derived directly from the instantaneous data rate of wirelessly received data after a one-time normalization calibration. (**e**) Compound action potential thresholds measured before and after the current-extraction experiment shown in **b**.

In any implanted sensing system, communication is essential to convey sensed information to the external world. Here we integrated a wireless radio transmitter that, through the use of extensive leakage power–reduction techniques[24], consumed a standby power of 46 pW at 0.9 V, which is at least an order of magnitude lower than previous work[25,26]. The transmitter shared the on-board antenna with the wireless kick-start circuit to minimize the implant's physical volume. The output data rate was set by an integrated ring oscillator, and the system could operate at instantaneous data rates programmable from 100 kbps to 10 Mbps up to a 1-m distance. Combined, the active energy consumption, packet length and standby power dictate the maximum frequency of packet transmissions. With the given power budget, the transmitter spent ~0.0001% of its time in active mode.

The chip was fabricated in a standard complementary metal-oxide semiconductor (CMOS) process with a minimum feature size of 0.18 µm, and it occupied a total volume of 2.4 × 2.4 × 0.2 mm^3. The chip was wire-bonded to a printed circuit board prototype (**Fig. 3a**) that is currently sufficiently small to be implantable in the human mastoid cavity, or in the bulla cavity of cats, gerbils or chinchillas (**Fig. 1**)[27].

We operated the chip for up to 5 h using the EP of an anesthetized Hartley Albino *Cavia porcellus* (guinea pig) as the source of energy into the system, after an initial wireless kick-start. Because these were feasibility studies, the electrode tips were inserted into the cochlea and the electrode shafts were connected to the endoelectronics chip located outside the guinea pig rather than implanted in the middle ear (**Supplementary Fig. 1**). **Figure 3b** shows the C_{supply} system supply voltage, V_{supply}, which replenished and persisted throughout a 20-min measurement (**Supplementary Fig. 2** shows the results from a 5-h experiment). As the system operated longer than the energy contained in the initial kick-start otherwise permitted (6 min), these results demonstrate an energy-harvesting system powered primarily from a mammalian electrochemical potential. The boost converter's average input impedance was configured to approximately equal the electrode impedance, so the converter extracted close to the maximal possible power from the EP given the physical constraints of the electrodes. As a result, V_{supply} slowly fluctuated as the animal's EP, and therefore the available energy into the system, varied. On a smaller timescale, as shown in **Figure 3c** for three different experiments, V_{supply} periodically dropped by 36–48 mV during active-mode wireless transmissions. After the voltage drop, the boost converter continued to harvest energy from the EP by trickle-charging capacitor C_{supply}, thereby recovering energy spent during the transmission.

We used energy harvested from the EP not only to power a wireless transmitter but also to sense relative changes in the EP after the voltage drop seen in the electrode resistance (V_{IN}). Because the instantaneous radio data rate was generated internally by a ring oscillator whose frequency varied with V_{supply} (which in turn varied with the EP and therefore V_{IN}), the wirelessly received data bits were inherently encoded with EP information. Thus, by monitoring the output data rate, we demonstrated that this self-powered system was also capable of continuously monitoring relative changes in the EP (**Fig. 3d**). Trends in sensed V_{IN} (equal to $V_{EP}R_{in,eff}/(R_{in,eff} + R_{elec})$), powered by the EP, were within a 0.45-mV r.m.s. error of direct measurements by an external battery-powered device over a 2.5-h experiment.

To test whether the system affected hearing, we measured compound action potential thresholds before and after electrode insertion (**Supplementary Fig. 3**) and before and after current draw (**Fig. 3e**) in two different anesthetized guinea pigs, respectively. Because the cochlea is tonotopically organized, with the high frequencies encoded at the cochlear base and low frequencies encoded at the cochlear apex, we tested cochlear function along its length by using tone pips of different frequencies. Insertion of the beveled glass microelectrodes did not adversely affect hearing (**Supplementary Fig. 3**). Likewise, current draw during the experiment shown in **Figure 3b** had essentially no effect on hearing for frequencies up to 16 kHz (**Fig. 3e**). A small

degradation in threshold was observed at a frequency of 23 kHz, which is encoded close to the round window (near the cochlear base). This degradation is probably due to the electrode tip, which was designed to be ~2 µm in diameter after beveling so as to allow low electrode impedance, typically ~800 kΩ, which is required for energy extraction from the EP. At such sizes, electrodes can cause local physical trauma to the cells lining the basilar membrane and thereby allow leakage of ions across the endolymph-perilymph barrier as well as leakage of ions from the fluid-filled electrodes into cochlear fluids. In contrast, electrodes that have been used to stably record the EP for many hours have tips <1 µm in diameter and impedances >5 MΩ[28]. Together, our data imply that major improvements in low-impedance, small-diameter electrode design would be required to allow long-term energy extraction from the EP without causing long-term cellular trauma during electrode insertion. In the meantime, our prototype system demonstrates feasibility with minimal effect on hearing in the short term.

With future miniaturization of low-impedance electrode tips and with refinements in minimally invasive surgical approaches to endolymph (for example, via Reissner's membrane[29]), our system would be useful in animal studies and could find eventual applications in human biotechnology and medicine. Small rodents are commonly used in hearing research, and our proposed energy-harvesting system could enable miniaturized and fully implantable sensing devices with minimal risk of malfunction from external infections or trauma. We envision using chemical and other electronic sensors and actuators not only in the cochlea and the nearby vestibular end organs of the inner ear (**Fig. 1**) but also in adjacent structures such as the temporal lobe of the brain, the facial nerve and the carotid artery, all of which are within millimeters of the cochlea in humans and rodents.

In the future, energy extraction from the cochlea may be applicable to humans. Surgical insertion of devices such as cochlear implants and stapes prostheses into the human inner ear is already possible with minimal risks of damaging normal or residual hearing[30,31]. Although the risk of hearing loss is higher when inserting an electrode into endolymph rather than perilymph, there are many forms of deafness in which the EP is normal, such as deafness due to loss of sensory cells, cochlear neurons or supporting cells. In such cases, the benefit of a battery-less system for sensing of key molecules in the inner ear may outweigh the potential risk to the EP during electrode insertion into endolymph. Although we have identified and overcome key challenges in developing the components of the system necessary to harvest net positive energy from the inner ear for hours at a time, important future work is required in electrode miniaturization and surgical approaches in order to advance from demonstrating feasibility to integrating all components into a safe, fully implantable system for long-term operation.

METHODS

Methods and any associated references are available in the online version of the paper.

Note: Supplementary information is available in the online version of the paper.

ACKNOWLEDGMENTS

We acknowledge support from the C2S2 Focus Center and the Interconnect Focus Center, two of six research centers funded under the Focus Center Research Program (FCRP), a Semiconductor Research Corporation entity (A.P.C., P.P.M., S.B.), and from US National Institutes of Health grants K08 DC010419 (K.M.S.) and T32 DC00038 (A.C.L.) and the Bertarelli Foundation (K.M.S.). We thank J.J. Guinan Jr. for experimental assistance and advice, and B. Zhu for preliminary studies.

AUTHOR CONTRIBUTIONS

A.P.C. and K.M.S. conceived the project. P.P.M., A.C.L., S.B., A.P.C. and K.M.S. designed experiments. P.P.M., A.C.L. and S.B. performed the experiments. P.P.M. and S.B. designed and implemented the electronic chip. A.C.L. performed the EP measurements. P.P.M., A.C.L., S.B., A.P.C. and K.M.S. wrote and edited the manuscript.

COMPETING FINANCIAL INTERESTS

The authors declare no competing financial interests.

Published online at http://www.nature.com/doifinder/10.1038/nbt.2394.
Reprints and permissions information is available online at http://www.nature.com/reprints/index.html.

1. Von Bekesy, G. Resting potentials inside the cochlear partition of the guinea pig. *Nature* **169**, 241–242 (1952).
2. Hibino, H., Nin, F., Tsuzuki, C. & Kurachi, Y. How is the highly positive endocochlear potential formed? The specific architecture of the stria vascularis and the roles of the ion-transport apparatus. *Pflügers Arch.* **459**, 521–533 (2010).
3. Himes, C., Carlson, E., Ricchiuti, R.J., Otis, B.P. & Parviz, B.A. Ultralow voltage nanoelectronics powered directly, and solely, from a tree. *IEEE Trans. NanoTechnol.* **9**, 2–5 (2010).
4. Rasmussen, M., Ritzmann, R.E., Lee, I., Pollack, A.J. & Scherson, D. An implantable biofuel cell for a live insect. *J. Am. Chem. Soc.* **134**, 1458–1460 (2012).
5. Halámková, L. *et al.* Implanted biofuel cell operating in a living snail. *J. Am. Chem. Soc.* **134**, 5040–5043 (2012).
6. Hochbaum, A.I. *et al.* Enhanced thermoelectric performance of rough silicon nanowires. *Nature* **451**, 163–167 (2008).
7. Qin, Y., Wang, X. & Wang, Z.L. Microfibre–nanowire hybrid structure for energy scavenging. *Nature* **451**, 809–813 (2008).
8. Chaudhuri, S.K. & Lovley, D.R. Electricity generation by direct oxidation of glucose in mediatorless microbial fuel cells. *Nat. Biotechnol.* **21**, 1229–1232 (2003).
9. Rapoport, B.I., Kedzierski, J.T. & Sarpeshkar, R. A glucose fuel cell for implantable brain-machine interfaces. *PLoS One* **7**, e38436 (2012).
10. Starner, T. & Paradiso, J.A. Human-generated power for mobile electronics. in *Low Power Electronics Design* (ed. Piquet, C.) 1–35 (CRC Press, 2004).
11. Donelan, J.M. *et al.* Biomechanical energy harvesting: generating electricity during walking with minimal user effort. *Science* **319**, 807–810 (2008).
12. Bullen, R.A., Arnot, T.C., Lakeman, J.B. & Walsh, F.C. Biofuel cells and their development. *Biosens. Bioelectron.* **21**, 2015–2045 (2006).
13. Dallos, P. Some electrical circuit properties of the organ of Corti. I. Analysis without reactive elements. *Hear. Res.* **12**, 89–119 (1983).
14. Takeuchi, S., Ando, M. & Kakigi, A. Mechanism generating endocochlear potential: role played by intermediate cells in stria vascularis. *Biophys. J.* **79**, 2572–2582 (2000).
15. Lang, H., Schulte, B.A. & Schmiedt, R.A. Endocochlear potentials and compound action potential recovery: functions in the C57BL/6J mouse. *Hear. Res.* **172**, 118–126 (2002).
16. Zidanic, M. & Brownell, W.E. Fine structure of the intracochlear potential field. I. The silent current. *Biophys. J.* **57**, 1253–1268 (1990).
17. Fernandez, C. Dimensions of the cochlea (guinea pig). *J. Acoust. Soc. Am.* **24**, 519–523 (1952).
18. Swanson, R.M. & Meindl, J.D. Ion-implanted complementary MOS transistors in low-voltage circuits. *IEEE ISSCC Dig. Tech. Papers* 192–193 (1972).
19. Chen, P.-H. *et al.* A 95mV-startup step-up converter with V_{TH}-tuned oscillator by fixed-charge programming and capacitor pass-on scheme. *IEEE ISSCC Dig. Tech. Papers* 216–217 (2011).
20. Ramadass, Y.K. & Chandrakasan, A.P. A battery-less thermoelectric energy harvesting interface circuit with 35mV startup voltage. *IEEE J. Solid-State Circuits* **46**, 333–341 (2011).
21. Shimamura, T. *et al.* Nano-watt power management and vibration sensing on a dust-size batteryless sensor node for ambient intelligence applications. *IEEE ISSCC Dig. Tech. Papers* 540–541 (2010).
22. Wieckowski, M., Chen, G.K., Seok, M., Blaauw, D. & Sylvester, D.D. A hybrid DC-DC converter for sub-microwatt sub-1V implantable applications. *IEEE Symposium on VLSI Circuits* 166–167 (2009).
23. Zhang, F. *et al.* A batteryless 19uW MICS/ISM-band energy harvesting body area sensor node SoC. *IEEE ISSCC Dig. Tech. Papers* 298–299 (2012).
24. Roy, K., Mukhopadhyay, S. & Mahmoodi-Meimand, H. Leakage current mechanisms and reduction techniques in deep-submicrometer CMOS circuits. *Proc. IEEE* **91**, 305–327 (2003).
25. Chen, G. *et al.* A cubic-millimeter energy-autonomous wireless intraocular pressure monitor. *IEEE ISSCC Dig. Tech. Papers*, 310–311 (2011).
26. Chow, E.Y., Chlebowski, A.L. & Irazoqui, P.P. Mixed-signal integrated circuits for self-contained sub-cubic millimeter biomedical implants. *IEEE Trans. BioCAS* **4**, 340–349 (2010).
27. Mason, M.J. Middle ear structures in fossorial mammals: comparison with non-fossorial species. *J. Zool. (Lond.)* **255**, 467–486 (2001).
28. Mills, D.M., Norton, S.J. & Rubel, E.W. Vulnerability and adaptation of distortion product otoacoustic emissions to endocochlear potential variation. *J. Acoust. Soc. Am.* **94**, 2108–2122 (1993).
29. Von Bekesy, G. DC resting potentials inside the cochlear partition. *J. Acoust. Soc. Am.* **24**, 72–76 (1952).
30. Fayad, J.N., Semaan, M.T., Meier, J.C. & House, J.W. Hearing results using the Smart piston prosthesis. *Otol. Neurotol.* **30**, 1122–1127 (2009).
31. Mowry, S.E., Woodson, E. & Gantz, B.J. New frontiers in cochlear implantation: acoustic plus electric hearing, hearing preservation, and more. *Otolaryngol. Clin. North Am.* **45**, 187–203 (2012).

ONLINE METHODS

Surgical procedures were performed at the Massachusetts Eye and Ear Infirmary with the approval of the Institutional Animal Care Committee (protocol no. 09-09-026). Animals were anesthetized and experiments were conducted in a heated, acoustically insulated chamber. Most animals had spontaneous, natural breathing. Mechanical ventilation was used only if respiration faltered owing to anesthesia. The auricle and neighboring musculature were reflected ventrally to expose the external auditory meatus and bulla. The lateral wall of the bulla, up to the caudal edge of the tympanic ring, was removed to allow visualization of and access to the round window. Pulled glass microelectrodes, mounted on micromanipulators, were advanced through the round window to access the fluid spaces of the inner ear. The negative electrode was inserted into the perilymph-filled scala tympani, and the positive electrode was inserted through the basilar membrane and sensory epithelium into the endolymph-filled scala media (**Supplementary Fig. 1**). Microelectrodes were pulled from Borosil capillary tubing (FHC). The tips of electrodes were beveled at a 25° angle using a BV-10 Microelectrode Beveler (Sutter Instruments) to achieve tip diameters of ~2 µm and electrode impedance of ~400–800 kΩ for both electrodes. Electrodes were mounted in half-cell holders containing Ag/AgCl exchange pellets (World Precision Instruments). Electrolyte composition was 2 M KCl. All circuit grounds were with reference to perilymph.

We constructed tone-pip audiograms by presenting brief tones (3.0-ms duration, 0.5-ms rise and fall times), at half-octave spacing between 2 and 32 kHz, to the external ear canal of the surgically targeted ear. The resulting compound action potential was recorded with a metal-wire electrode placed adjacent to the round window. The threshold was defined as the minimum sound intensity required to elicit a response above 10 µV (the noise floor was measured to be approximately 4 µV).

The printed circuit board was manufactured with an FR-4 substrate, and the chip and two capacitors were mounted on the top of the board, whereas the inductor was mounted on the bottom. The chip was encapsulated by a nonconductive epoxy for mechanical stability (not shown in **Fig. 3a** for clarity). The system supply voltage was measured during *in vivo* experiments with a Keithley 2602 SourceMeter, and V_{IN} was measured with an Agilent U1253A instrument set to 1 GΩ input impedance. A wireless receiver, built with discrete components, was used to down-convert and record the instantaneous transmitter data rate on a Tektronix TDS3064B oscilloscope. The chip power consumption was measured during characterization experiments with a Keithley 6430 SourceMeter and high-isolation triaxial cables for accurate low-current measurements.

The chip was initialized with a wireless kick-start from an external radio frequency source operating at 2.4 GHz placed several millimeters away for no more than 2 s. Owing to on-chip voltage clamps, capacitor C_{supply}, which had a capacitance of 200 nF, charged to at most 1.4 V during initialization. At 1.4 V, capacitor C_{supply} stored $E = 0.5C_{supply}V_{supply}^2 = 200$ nJ of energy. During operation, the boost converter, radio and peripheral circuits consumed 573 pW (at 0.9 V). At this power consumption, the circuit would theoretically operate for at most 6 min before completely exhausting the energy stored on capacitor C_{supply}; in practice, time to exhaustion is typically much shorter. Therefore, any experiment lasting longer than a few minutes extracted energy from the EP.

doi:10.1038/nbt.2394